Available online at www.sciencedirect.com
ScienceDirect
Trans. Nonferrous Met. Soc. China 23(2013) 3002−3010
Transactions of Nonferrous Metals Society of China
www.tnmsc.cn

Wrinkling prediction in rubber forming of Ti-15-3 alloy

Yong-na SUN, Min WAN, Xiang-dong WU

School of Mechanical Engineering and Automation, Beihang University, Beijing 100191, China

Received 21 September 2012; accepted 29 December 2012

Abstract: Wrinkling is a common failure in the sheet metal forming of titanium owing to the relatively poor ability to shrink. It is important to predict wrinkling accurately in the sheet metal forming without costly trials. The ABAQUS/Explicit code was utilized to predict the wrinkling behavior in the sheet metal forming of Ti-15-3 alloy sheets. In terms of the comparison of wrinkling behavior between the simulation and experiment of the Fukui's conical cup tests at room temperature, the sensitivities of wrinkling simulation to various input parameters were evaluated comprehensively and quantitatively. Prediction of wrinkling and influence of rubber hardness on the winkling behavior in the rubber forming of convex flange were investigated quantitatively and validated by the rubber forming experiments. The excellent agreements between the simulations and the experiments confirmed the accuracy of the prediction.

Key words: Ti-15-3 alloy; wrinkling; convex flange; rubber forming; quantitative analysis

1 Introduction

Metastable β-phase titanium alloys are the best candidates for aerospace application owing to their high specific strength, good hardenability and corrosion resistance. Ti−15V−3Al−3Cr−3Sn alloy (Ti-15-3) is a kind of metastable β-phase titanium alloy that has advantages of excellent cold deformability and ability to be aged to high strength [1,2]. Furthermore, it reduces the cost requirements when Ti-15-3 alloy deformed at room temperature [2,3]. Nevertheless, the cold sheet metal forming process and application of Ti-15-3 alloy are still at research stage, mainly owing to its inherent low plasticity [3,4].

Flanging with a convex edge is one of the basic types of flanges, which is much more complex, much more common and much less investigated than the straight flanging. The compressive strain happens in the circumferential direction because the arc length of the final flange is smaller than that of the original. The greater the flange length is, the larger the amount of compression is [5]. When the compressive strain achieves or exceeds a critical value, the local buckling of sheet metal occurs, which results in wrinkling. Studies on wrinkling in the convex flange have been focused on factors of exclusive Ti-15-3 alloy, such as tool geometry, blank geometry and material properties [6,7]. Wrinkling is one of the main failure modes in the stamping of sheet metal. And it is becoming more prevalent in the forming process owing to the great usage of high strength sheet metals in recent years [8,9]. Moreover, the onset of wrinkling in the convex flange, always referred as wall-wrinkling, is usually easier than the wrinkling in the flat flange since the relatively unsupported of the tool [9]. However, wrinkling is undesired for the final product [9,10]. Therefore, it is extremely important to predict and prevent wall-wrinkling in sheet metal forming of Ti-15-3 alloy. Unfortunately, the study on the failure in the cold forming of Ti-15-3 alloy is rarely found, if any, in literatures.

Rubber forming is always used for cold forming of titanium flanges [4]. Rubber forming, with a rubber pad contained in a rigid box acts as a punch, only requires a single metallic die/punch. The main attraction of rubber forming is its simplicity. Furthermore, rubber forming can diminish the forming procedure, shorten the production preparation cycle, lessen the springback and improve the surface quality [6,11]. And in the rubber forming process, the rubber hardness is the most concerned process parameter that must be detailed studied [12].

Recently, the finite element method (FEM) has been ever-increasing widely used to simulate sheet metal

Corresponding author: Min WAN; Tel/Fax: +86-10-82338788; E-mail: mwan@buaa.edu.cn
DOI: 10.1016/S1003-6326(13)62827-7

forming and plays an important role in quality control and problem analysis. But FEM concerning the rubber forming process is relatively backward and unbalanced compared with its development in the traditional sheet metal forming process with rigid die, owing to the complicated deformation of rubber [12,13]. Nevertheless, a few numerical investigations of rubber forming process can be found in literatures.

GIUSEPPE [6] and ALBERTI et al [14] respectively optimized the rubber forming process by numerical simulations. Their investigations exposed the effectiveness of FEM in rubber forming process design, but did not consider the influence of rubber hardness and wrinkling behavior. RAMEZANI et al [15] and PRETE et al [16] conducted FEM studies concerning the rubber forming process and investigated the influence of rubber hardness on stress distribution in the sheet. However, a detailed study of wrinkling analysis in the convex flange was also ignored in these works. These weaknesses necessitated the finite element analysis of the influence of rubber hardness on wrinkling in the rubber forming of convex flange, with accurate results and reduced cost.

FEM with either an implicit or explicit integration method can be utilized for sheet metal forming simulation. But the implicit method has difficulty in predicting wrinkling phenomenon without initial imperfections, and frequently experiences convergence problems. Contrarily, the explicit method can shape wrinkles automatically thanks to the accumulation of numerical error. Additionally, the explicit method has advantage of requiring very small time increments, but for quasi-static forming process, it may lead to extreme computation time. However, the onset and growth of wrinkle simulated by the explicit integration method is sensitive to the input parameters, such as mesh density and simulation speed [10,17]. KAWKA et al [17] reported the important effect of mesh shape on wrinkles, but this investigation was limited to the distribution and shape of wrinkles. WANG et al [18] simulated the wrinkles' wavelength and amplitude, but introduced the out-of-plane disturbing forces. Even so, FEM was still of significance in industrial designs, for instance, the elimination of wrinkling in motor cycle oil tank [19].

In previous work, numerical factors influencing wrinkling simulation have not been evaluated comprehensively and quantitatively, although the effect of each individual factor was roughly understood. It still required a burdensome trial-and-error process for setting-up before the complicated forming simulations. To overcome these drawbacks, wrinkling which occurred in the drawing of Fukui's conical cups was analyzed numerically and experimentally. The Fukui's conical cup test was utilized mainly owing to its simple component geometry enabled the easy comparison of FEM and experimental results. Additionally, wrinklings in the convex flange and in the wall of conical cup were consistently originated from the compressive circumferential stresses [20]. Consequently, the investigation of wrinkling in the Fukui's conical cup was complicated enough to provide some general conclusion available for wrinkling prediction in the rubber forming of convex flange.

In this work, wrinkling of the Ti-15-3 alloy sheet during the Fukui's conical cup forming test was quantitatively investigated. Utilizing the foundational problems with commonness in the simulation of conical cup, wrinkling behavior in the convex flange manufactured by rubber forming was predicted. And effects of rubber hardness on the wrinkling were quantitatively described and experimentally validated.

2 Fukui's conical cup test

Fukui's conical cup tests were performed on circular specimens (16 mm in diameter, 1.0 mm in thickness) according to GB/T15825.6—2008 Standard at 0.5 mm/s strain rate. Before experiment, the rolling direction of the sheet was marked by a line, and interface between the sheet and the die was lubricated. Experiments were carried out on the BCS 50 press machine.

As shown in Fig. 1, there are two wrinkles in the side wall, they are in the direction along (Marked as X1 and X2) and perpendicular (Marked as Y1 and Y2) to the rolling direction of the sheet, respectively. It can be seen that the generatrix shape of conical cup is no longer straight. The wrinkles' wavelength and height along the cup edge and the distance from the edge to wrinkles' are measured quantitatively. Table 1 presents the measurements of wrinkles in concial cup test.

Fig. 1 Wrinkled conical cup

Table 1 Measurements of wrinkles in conical cup test

Wrinkle	Wavelength/mm	Height/mm	Distance/mm
X1	1.68	10.46	2.68
X2	1.54	11.18	2.54
Y1	3.72	9.56	4.72
Y2	3.64	8.24	4.64

It comes to a conclusion that Ti-15-3 alloy has poor performance in complex forming operations including

drawing and bulging. This instability phenomenon is caused by both the high strength property of Ti-15-3 alloy and the relatively unsupported of the wall.

3 FEM simulation of conical cup test

3.1 FEM modeling of conical cup test

The Fukui's conical cup test was simulated by the ABAQUS/Explicit. In the finite element simulations, the forming tools were modeled as rigid bodies, correspondingly the S4R rigid shell elements were used only to define the tooling geometry and were not for the stress analysis. The sheet metal was defined as deformable and meshed by the 4-node shell elements with reduced integration (S4R). Simultaneously, the enhanced hourglass control approach was chosen to avoid excitation of hourglass modes.

The plasticity of the Ti-15-3 alloy was directly imported from tension test results prepared according to GB/T228—2002 standard. The elastic-plastic material model with in-plane anisotropy yield condition and classical isotropic hardening was used. The anisotropy was described by Hill's 1948 yield criterion [21], and in which the material constants F, G, H, L, M, N (stress ratios in ABAQUS/Explicit) were calculated based on Lankford's. Coefficients of r_0, r_{45} and r_{90} were 0.9423, 0.757 and 1.1423, respectively [22].

The pure master-slave contact algorithm was utilized to simulate contact between rigid tools and the sheet surfaces. And the penalty function algorithm was utilized to model the friction behavior. The friction coefficient between the sheet and the die was 0.27; friction coefficient between the sheet and the punch was 0.45. The corresponding model with appropriate boundary conditions was established. And the punch went with smooth type amplitude.

3.2 Determination of punch velocity

In this quasi-static problems, the way of dealing with different velocities was equivalent to the same displacement of punch but with different step time. The supposed punch speeds were presented in Table 2. And simulations were conducted without mass scaling.

Table 2 Comparison of various velocity in simulation of conical cup test

Scheme	Velocity/(mm·s^{-1})	h/mm	t/s	Number
FE-1	50000	−	212	0
FE-2	5000	15.88	536	4
FE-3	1000	14.92	2358	5
FE-4	500	13.95	3660	5
FE-5	50	12.01	1.7×10^6	1
Experiment	0.5	−	44	4

In order to determine the onset of wrinkling, the strain history of elements in the wall of the conical cup was examined at each increment. Figure 2 shows the plot of major and minor principal strain of an element versus punch stroke. It is noticed in Fig. 2 that the difference of the major and minor principal strains increases abruptly when the punch stroke is 15.88 mm, which implies a dramatic shape change. A particular review of the deformed shape change at this moment confirms that wrinkles are shaped, as shown in Fig. 3. Before this time, no wrinkle appears.

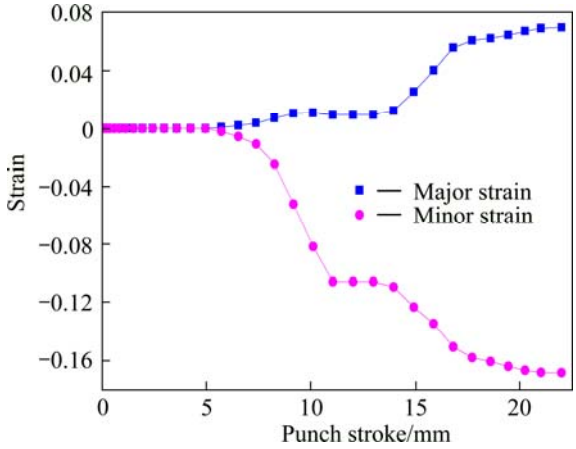

Fig. 2 Strain history of element in wrinkling zone

Fig. 3 Wrinkle formation with punch stroke of 15.88 mm

Wrinkles in the side wall were obviously draw-wall wrinkles because there was no support of die surface in this area. The sheet metal in this area was pulled in the direction of the punch advancing and was compressed in the circumference direction. These two directions were also the principal directions. As shown in Fig. 2, the abrupt change of the principal strains in these two direction indicates that the dramatic increase of compressive hoop strain leads to the formation of wrinkles.

Based on the history of compressive hoop strain of different elements, the abrupt change of compressive

hoop strain was set as the wrinkling onset criterion. The punch stroke (h) when wrinkling appears, the computation time (t) and the number of wrinkles are listed in Table 2. And the simulation results are shown in Fig. 4.

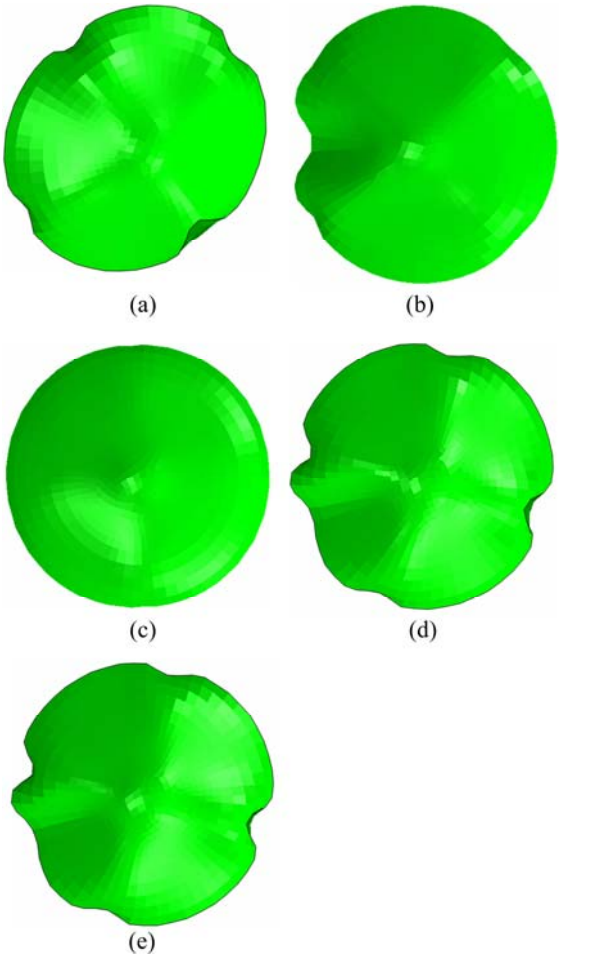

Fig. 4 Wrinkling results at different velocities: (a) 5000 mm/s; (b) 50 mm/s; (c) 50000 mm/s; (d) 500 mm/s; (e) 1000 mm/s

Table 2 and Fig. 4 demonstrate that the results are different although computed by the same FEM model with same geometry, mesh, material model and boundary conditions.

As shown in Fig. 4(a), the wrinkles' distribution and shape appeared to be adequate to the experimental result when velocity was 5000 mm/s. It demanded an extreme computation time about 106 s when the velocity was 50 mm/s, which was increased artificially to 100 times of the experiment. This computation time could not express the high efficiency of the FEM enough. And in this case, the wrinkling onset was earlier (h=12.01 mm), as the punch advanced, the wavelength decreased and the height increased, and there was only 1 wrinkle, as shown in Fig. 4(b). But the excessive increased velocity, such as 50000 mm/s, might delay the onset of wrinkling, even suppress, as shown in Fig. 4(c). Although the computation time was accepted when the velocity was 500 or 1000 mm/s, the distribution and the number of wrinkles conflicted with the experimental results as shown in Figs. 4(d) and (e), respectively.

The main reason which comes to mind is the difference of punch speed, which can be amplified by an excessive speed in the simulation. The computation time is in proportion to the step time, even for such simple model as Fukui's conical cup.

To summarize, velocity of 5000 mm/s is the best choice in the simulation of wrinkling of the Ti-15-3 alloy sheet during the conical cup forming test.

3.3 Determination of mesh density

Meshes of the sheet were relatively smaller than that of rigid tools to improve efficiency and accuracy of simulation. The sheet was divided as division of contact with punch and side wall area, and different mesh densities were distributed in different divisions. The discretization in the side wall was the research priority and refined adequately.

To investigate the influence of mesh density, three levels of element size in the radial direction and circumference in the side wall area were specified in Table 3. The sheets were discretized by Hypermesh 9.0.

Table 3 Levels of element size in simulation of conical cup test

Level	Circumference/mm	Radius/mm
1	2	2
2	3	3
3	4	4

As shown in Fig. 5, the shape of bulges is irregular. Therefore, it is difficult to describe bulges quantitatively. Table 4 presents the differences between the simulations and experiments, in terms of the shape and number of the bulges. It can be concluded that the schemes 3−5 are feasible.

Figures 5(a), (b) and (c) illustrate that there are 4 wrinkles accompanied by some buckling when the circumference is 2 mm; and there are also 4 wrinkles when the circumference is 3 mm; whereas, there are only 2 wrinkles when circumference is 4 mm meanwhile the radius is 2 or 3 mm; but wrinkling is invisible when element size is 4 mm in both direction.

Although it clearly proves that wrinkles are very sensitive to the initial element size in Fig. 5, it cannot pronounce the accurate mesh density. So, a quantitative analysis of the wrinkles' wavelength, wave height and distance from the cup edge to the their disappear were conducted. And the detailed examination were focused on FEM schemes 3−6. The errors were defined as

Table 4 Wrinkling number and bulges in simulation of conical cup test with various element sizes

Scheme	Circumference/mm	Radius/mm	Wrinkling number	Difference of bulges from experiment
1	2	2	2	1 bulge less, 2 depressed more in rolling direction
2	2	3	2	1 bulge less, 1 depressed more in rolling direction
3	2	4	4	Similar
4	3	2	4	Similar
5	3	3	4	Similar
6	3	4	4	Larger
7	4	2	4	1 depressed more in rolling direction
8	4	3	4	Larger in rolling direction, 1 depressed more
9	4	4	4	Larger in rolling direction, 1 depressed more

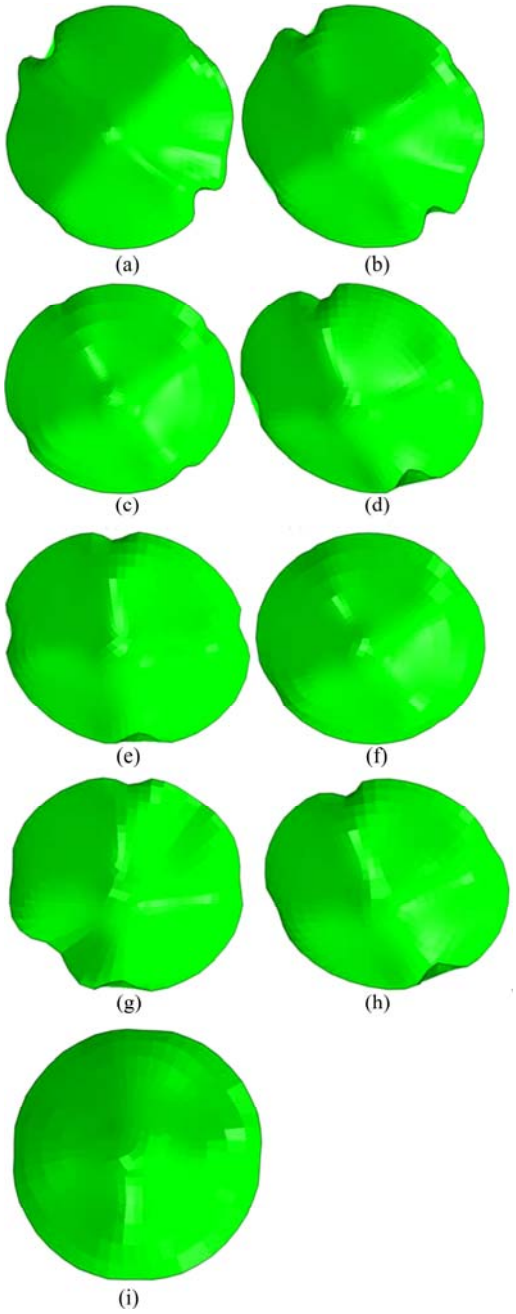

Fig. 5 Wrinkling distribution of different mesh densities: (a) Scheme 1; (b) Scheme 2; (c) Scheme 3; (d) Scheme 4; (e) Scheme 5; (f) Scheme 6; (g) Scheme 7; (h) Scheme 8; (i) Scheme 9

measurements of experimental results subtracted from FEM results and presented in Fig. 6.

Figure 6 shows the dependence of wrinkle behavior on the element size. The scheme 5 with element size of 3 mm×3 mm is most applicable to predict side wall wrinkling in the stamping of Ti-15-3 alloy, although there are still some minor errors.

4 Wrinkling in rubber forming of convex flange

In this work, the rubber forming, with a rubber pad contained a rigid chamber, was employed to stamp the Ti-15-3 alloy sheet component. The component has a convex flange, and the geometric of the flange is with convex radius of 140 mm, bend angle of 90° and circumferential angle of 94°. And the external radius of the blank is 155 mm. The chamber is geometrically characterized by a diameter of 240 mm and a height of 210 mm. The schematic diagram of the experimental set-up is shown in Fig. 7.

4.1 FEM modeling of rubber forming

The quasi-static non-linear approach with negligible temperature effects is assumed for this study. In the rubber forming process, rubber has nonlinear stress-strain characteristics for relatively large deformations. Generally it is assumed as isotropic and nearly incompressible. To model this hyper-elastic material, ABAQUS adopts a constitutive law based on total strain energy density U. There are several forms of strain energy potentials available in ABAQUS: the Mooney-Rivlin form, the neo-Hookean form, the polynomial form and the Yeoh form, etc. In addition, when experimental test data are available (typically, this requires at least uniaxial data), ABAQUS/CAE can automatically evaluate the hyper-elastic material behavior to determine the optimal strain energy potential by creating response curves without specifying a particular strain energy potential.

As a reduced polynomial model, the Mooney-Rivlin model uses a strain energy potential U, whose derivative

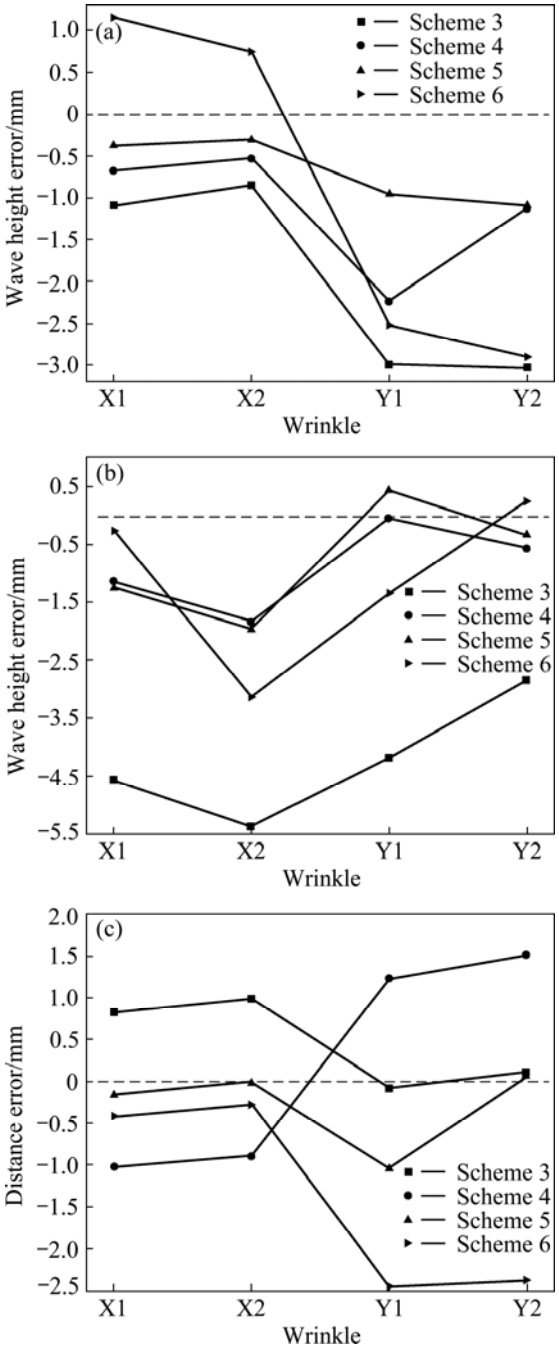

Fig. 6 Quantitative comparison of wrinkles between FEM and experimental results: (a) Error of wave height; (b) Error of wavelength; (c) Error of distance

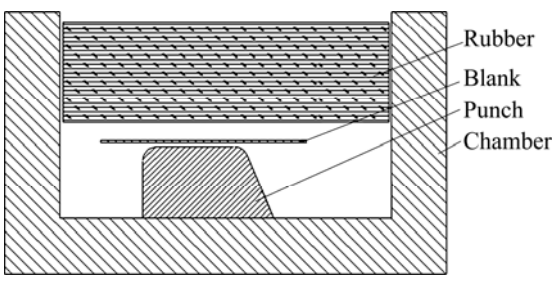

Fig. 7 Schematic representation of experimental set-up

with respect to a strain component determines the corresponding stress component. The form of the Mooney-Rivlin strain energy potential is

$$U=\sum_{i+j=1}^{N} C_{ij}\left(I_1-3\right)^i\left(I_2-3\right)^j+\sum_{i=1}^{N}\frac{1}{D_i}\left(J_{\mathrm{el}}-1\right)^{2i} \quad (1)$$

where U is the strain energy potential; J_{el} is the elastic volume ratio; I_1 and I_2 are measures of the distortion in the material; N, C_{ij}, and D_i are material constants, which may be functions of temperature. Commonly, two Mooney-Rivlin parameters (C_{10} and C_{01}) are used to describe hyper-elastic rubber deformation, which can be determined by experiments.

Three different hardness Shore A (70, 80, 90) of rubber were used in the FEM simulation to investigate the influence of rubber hardness on wrinkling in the convex flange. Tensile tests were performed according to GB/T528—2009 standard at 8 mm/s strain rate, which repetition was statistically meaningful. Compressive tests were performed on cylindrical specimens (12 mm in diameter, 10 mm in thickness) according to GB/T7757—93 standard at 0.2 mm/s strain rate. In this work, tests were conducted on the rubber of 70 and 90 Shore A hardness and used to construct response curves of polynomial models. As summarized in Fig. 8, the Mooney-Rivlin form was more accurate in fitting experimental results. Nevertheless, mechanical properties of Shore 80 A was from Ref. [23]. The parameters of rubber were listed in Table 5.

The rigid tools and the blank were defined same as in the conical cup simulations. Most of all, mesh sizes in the convex flange were 3 mm×3 mm. And C3D8R elements with visco-elastic hourglass control approach were used to the discretization of rubber pad. There were two different interfaces in the rubber forming. The penalty function algorithm was utilized to model the friction behavior.

The interfaces between the rubber and the metal, including sheet and rigid punch, were modeled using the general contact algorithm with a coefficient of friction of 0.15, while the interface between the rigid punch and the sheet using the pure master-slave contact algorithm with a coefficient of friction of 0.27. Boundary conditions were defined according to actual boundary conditions. And the forming loads were applied on the sheet in terms of pressure applied on the top surface of the rubber pad.

4.2 Simulation results and discussion

In the rubber forming process, the sheet deformed under the pressure of rubber. From the simulation results, it is clear to see that the rubber forming process contains three different stages: the first is the self-deformation of the rubber; the second is the deformation of the sheet metal under the press of rubber; the third stage is the

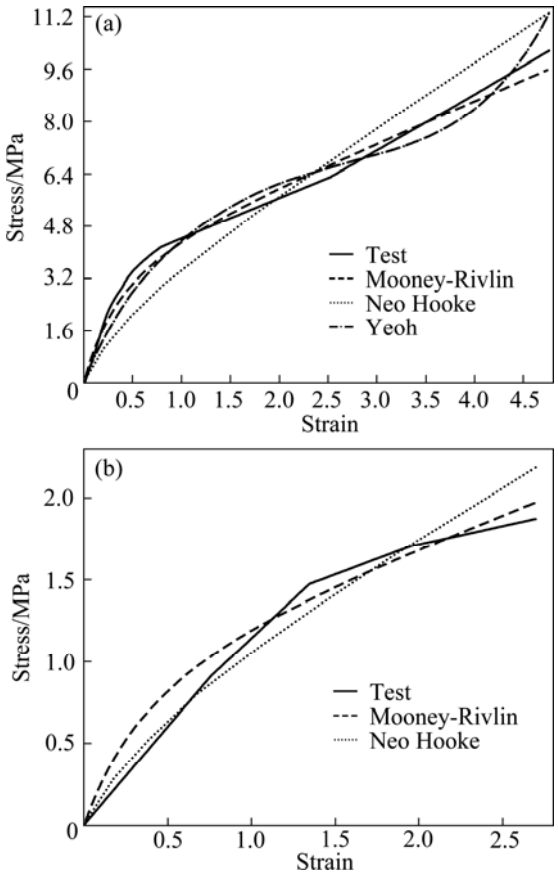

Fig. 8 Stress—strain curves of different hyper-elastic models: (a) Shore 70 A; (b) Shore 90 A

Table 5 Parameters of rubber material

Hardness Shore A	C_{10}	C_{01}
70	0.63	1.20
80	0.99	0.68
90	0.19	0.29

sheet metal complying with the shape of the rigid die. It also can be found that the defect in this forming process is the wrinkling in the convex flange because of the excessive compressive hoop strain and unsupported by the punch.

Figure 9 shows the distribution and shape of wrinkles in the convex flange resulting from rubber forming with various rubber hardness. Moreover, it is found that the distribution and shape of wrinkles are

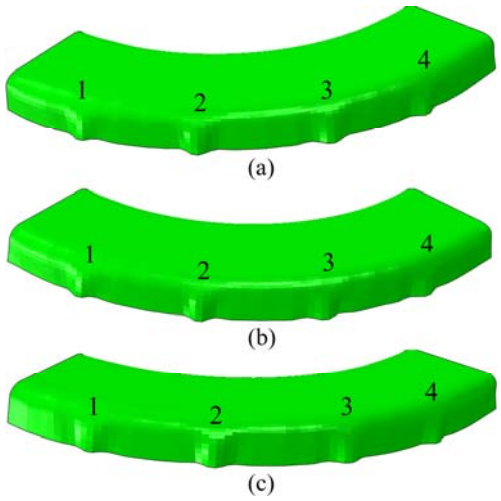

Fig. 9 Simulation results of wrinkling in rubber forming of convex flange with different rubber hardness: (a) Shore 70A; (b) Shore 80 A; (c) Shore 90A

nearly uniform. The distance of wrinkles in the convex flange is not considered in this work owing to wrinkles developed nearly from the bending corner to the top of the flange. A detailed examination of the wrinkles' wavelength and wave height was extracted from the FEM results and listed in Table 6.

It can be seen from Fig. 9 and Table 6 that the increment of rubber hardness results in the decrease of wave height and increase of wavelength. In other words, wrinkles become relative flat with the increase of rubber hardness. This indicates that the rubber with harder hardness is in favor of wrinkling elimination.

The reason is that although different hardness rubbers have nearly equivalent capability to transfer force in the close container, the pressure on the wrinkles are different owing to the various deformation ability of rubber. When the rubber hardness is relatively softer, the distribution of pressure on the wrinkles is nearly uniform. Therefore in this instance, higher pressure will increase the wave height and decrease the wavelength, so that wrinkles cannot be eliminated even if pressure is excessive. Nevertheless, when the rubber hardness is relatively harder, the distribution of pressure on the wrinkles is non-uniform and the pressure acting on the peak of the wrinkling is greater than that on the valley.

Table 6 Measurement of wrinkles in rubber forming of convex flange with different rubber hardness values

Hardness (Shore A)	Wrinkling 1		Wrinkling 2		Wrinkling 3		Wrinkling 4	
	Wavelength/mm	Height/mm	Wavelength/mm	Height/mm	Wavelength/mm	Height/mm	Wavelength/mm	Height/mm
70	8.75	2.78	8.51	2.96	8.91	2.71	9.16	2.79
80	9.17	2.52	10.86	2.60	10.48	2.63	10.84	2.65
90	9.26	1.34	11.21	1.35	11.58	1.30	11.76	1.35

Table 7 Comparison of wrinkles in rubber forming of convex flange between FEM and experiment with Shore A 90

Comparison	Wrinkling 1		Wrinkling 2		Wrinkling 3		Wrinkling 4	
	Wavelength/ mm	Height/ mm	Wavelength/ mm	Height/ mm	Wavelength/ mm	Height/ mm	Wavelength/ mm	Height/ mm
FEM	9.26	1.34	11.21	1.35	11.58	1.30	11.76	1.35
Experiment	8.58	1.28	11.02	1.42	11.50	1.38	11.52	1.26

Under this condition, the wave height verges to zero to eliminate the wrinkle with higher pressure. However, the wrinkle problem cannot be improved only by changing the rubber hardness owing to wrinkling in the convex flange are also affected by the geometric of punch and sheet material, etc.

4.3 Rubber forming experiments of Ti-15-3 alloy

In this work, rubber forming experiments were performed with the help of a hydraulic press YD28Q−550Q, equipped with a monitoring system which enabled the acquisition of information related to the process. The most advantage of the hydraulic press is that the ram velocity and load amount can be adjusted to the requirements of the deformation process.

In this experiment, a Shore 90 A hardness rubber was utilized to stamp the Ti-15-3 alloy sheet. Firstly, surfaces of the sheet and rigid punch were cleaned and lubricated before experiment to minimize friction. Then, the rigid punch was placed in the chamber and the Ti-15-3 alloy sheet was introduced between the rigid die and the flexible punch. After that, the stroke moved down at reasonable velocity applying pressure on the rubber, accordingly, caused the rubber deformed in the chamber to comply the blank with the rigid die.

The formed part with 4 wrinkles in the convex flange is shown in Fig. 10. It can be seen from Fig. 10 that the onset of wrinkles is nearly from the bending corner, which is almost as same as the FEM. Wrinkles' wavelength and wave height are measured, comparing with the simulation results, as demonstrated in Table 7.

Fig. 10 Rubber forming experimental wrinkles in convex flange with Shore A 90 rubber

According to Table 7, the simulation of distribution, number and shape of wrinkles shows excellent consistency with experiments although with minor errors, which may possibly be blamed on the measurement error. The prediction error of wrinklings 1 and 4 are relatively larger owing to the assumption of uniform in the FEM, variously, the experiment material has impurities. Although the wrinkling prediction error of wave height is larger than that of wavelength, the FEM prediction error is no more than 8%.

5 Conclusions

1) Ti-15-3 alloy has poor formability of complex forming operations. Wrinkling is the main failure which limits the comprehensive performance of drawing and bulging.

2) The sensitivities of wrinkling simulation to the input parameters are investigated. It is obvious that too fast velocity delays the onset of wrinkling, but too low velocity requires costly computational time. The velocity of 5000 mm/s is the best choice. And the element sizes of 3 mm×3 mm can predict wrinkles overwhelmingly accurate in the stamping of Ti-15-3 alloy sheet.

3) It is shown that the prediction of wrinkling in the rubber forming of convex flange matched well with the experimental results, although with minor error less than 8%. It suggests that the proposed method can be used to predict wall wrinkling in the stamping of Ti-15-3 alloy sheets.

4) In the rubber forming process of convex flange, the hardness of the rubber has a great influence on the wrinkles' wavelength and wave height to some extent, but has little influence on the wrinkles' distribution. Rubber with harder hardness is in favor of wrinkling diminution. However, it is difficult to achieve wrinkling elimination only by increasing the rubber hardness when the flange height is greater. For this convex flange, it is necessary to take further investigation to eliminate wrinkles in the rubber forming of Ti-15-3 alloy.

References

[1] ISMARRUBIE Z N, ALI A, SATAKE T, SUGANO M. Influence of microstructures on fatigue damage mechanisms in Ti-15-3 alloy [J]. Material & Design, 2011, 32: 1456−1461.

[2] ZHOU Zhong-bo, FEI Yue, LAI Min-jie, KOU Hong-chao, CHANG Hui, SHANG Guo-qiang, ZHU Zhi-shou, LI Jin-shan, ZHOU Lian. Microstructure and mechanical properties of new β type titanium alloy [J]. Transactions of Nonferrous Metals Society of China, 2012, 20(12): 2253−2258.

[3] SHAN D B, LU Y, LI P, XU Y. Experimental study on process of cold-power spinning of Ti-15-3 alloy [J]. J Mater Process Technol, 2001, 115(3): 380−383.

[4] BEAL J D, BOYER R, SANDERS D. Forming of titanium and titanium alloys [J]. Metalworking: Sheet Forming, 2006, 14: 656−669.
[5] ASNAFI N. On stretch and shrink flanging of sheet aluminum by fluid forming [J]. J Mater Process Technol, 1999, 96: 198−214.
[6] GIUSEPPE S. A numerical and experimental approach to optimise sheet stamping technologies: Part II-Aluminum alloys rubber-forming [J]. Mater Des, 2001, 22: 299−315.
[7] HU P, LI DY, LI Y X. Analytical models of stretch and shrink flanging [J]. International Journal of Machine Tools & Manufacture, 2003, 43: 1367−1373.
[8] NARAYANASAMY R, NARAYANAN S C. Wrinkling behaviour of interstitial free steel sheets when drawn through tapered dies [J]. Mater Des, 2007, 28: 254−259.
[9] MOHAMMAD A S, MAHMOUD A, MOSTAFA K. Investigation into wall wrinkling in deep drawing process of conical cups [J]. J Mater Process Technol, 2011, 211: 1783−1795.
[10] WANG X, CAO J. On the prediction of side-wall wrinkling in sheet metal forming processes [J]. International Journal of Mechanical Sciences, 2000, 42: 2369−2394.
[11] MAZIAR R, MOHD R Z, ROSLAN A. Computer aided modelling of friction in rubber-pad forming process [J]. J Mater Process Technol, 2009, 209: 4925−4934.
[12] PENG L, HU P, LAI X, MEI D Q, NI J. Investigation of micro/meso sheet soft punch stamping process-simulation and experiments [J]. Mater Des, 2009, 30: 783−790.
[13] DIRIKOLU M H, AKDEMIR E. Computer aided modeling of flexible forming process [J]. J Mater Process Technol, 2004, 148(3): 376−381.
[14] ALBERTI N, FORCELLESE A, FRATINI L, GABRIELLI F. Sheet metal forming of titanium blanks using flexible media [J]. CIRP Annals-Manufacturing Technology, 1998, 47: 217−220.
[15] RAMEZANI M, RIPIN Z M, AHMAD R. Numerical simulation of sheet metal stamping processing using flexible punch [J]. Proc IMechE, Part B: J. Engineering Manufacture, 2009, 223: 829−840.
[16] PRETE A D, PAPADIA G, MANISI B. Computer aided modelling of rubber pad forming process [J]. Key Eng Mater, 2011, 473: 637−644.
[17] KAWKA M, OLEJNIK L, ROSOCHOWKSKI A, SUNAGA H, MAKINOUCHI A. Simulation of wrinkling in sheet metal forming [J]. J Mater Process Technol, 2001, 109: 283−289.
[18] WANG C G, TAN H F, DU X W, WAN Z M. Wrinkling prediction of rectangular shell-membrane under transverse in-plane displacement [J]. Int J Solids Struct, 2007, 20: 6507−6516.
[19] CHEN K, LIAO Y CH. Analysis of draw-wall wrinkling in the stamping of a motorcycle oil tank [J]. J Mater Process Technol, 2007, 192−193: 283−289.
[20] WANG CH T, KINZEL G, ALTAN T. Wrinkling criterion for an anisotropic shell with compound curvatures in sheet forming [J]. Int J Mech Sci, 1994, 10: 945−960.
[21] HILL R. The mathematical theory of plasticity [M]. Oxford: Oxford University Press, 1998.
[22] SUN Yong-na, Wan Min, WU Xiang-dong. Study on friction coefficient in rubber forming process of Ti-15-3 alloy [J]. Transactions of Nonferrous Metals Society of China, 2012, 22(12): 3012-3-3018.
[23] YANG W J. Research on springback compensation method and rapid process preparation system for rubber fluid-cell forming process [M]. Beijing: Beihang University Press. (in Chinese)

Ti-15-3 钛合金橡皮成形凸弯边起皱预测

孙永娜，万 敏，吴向东

北京航空航天大学 机械工程及自动化学院，北京 100191

摘 要：基于 ABAQUS/Explicit 对 Ti-15-3 钛合金室温锥杯成形实验中悬空侧壁起皱现象进行分析，通过对零件边缘的皱纹波长和峰高的定量研究，获取较适合 Ti-15-3 钛合金室温成形侧壁起皱的模拟参数。将 Ti-15-3 钛合金室温锥杯成形起皱获取的模拟参数，用于 Ti-15-3 钛合金凸弯边橡皮成形起皱的预测，通过定量比较凸弯边边缘的皱纹波长和峰高，分析不同硬度的橡皮对 Ti-15-3 钛合金凸弯边橡皮成形起皱的影响。经实验验证，有限元模拟对 Ti-15-3 钛合金凸弯边上皱纹的模拟与实验结果有很好的一致性。

关键词：Ti-15-3 钛合金；起皱；凸弯边；橡皮成形；定量分析

(Edited by Chao WANG)